0.1 Drag force experiments

As we introduced in the last section of **Experimental approach** chapter, we used the full frequency sweep method for each of oscillators. Each point on following graphs was obtained by a pair of full frequency sweeps across the resonant value of given oscillator. One sweep was performed with increasing frequency and the second one with decreasing frequency, which made us confident that no hysteresis effect was present.

We present all the measurements in the form of typical hydrodynamic visualizations (velocity-force response, drag coefficients and appropriate dimensionless numbers) of oscillating wire, torsional disc and tuning fork, respectively.

0.1.1 Vibrating wire

We were measuring the voltage in phase with the driving current to obtain the resonant response. Above high enough applied drives ($\sim 0.8\,\mathrm{mA}$ at temperature $1.67\,\mathrm{K}$ responding in $\sim 0.1\,\mathrm{m/s}$ peak velocity), there was present a frequency shift and a *peak softening* effect. Together with a poor calibration of magnetic field produced by permanent magnets, the peak velocity on the wire top is known with the accuracy about $\pm 20\%$. Fortunately, this error doesn't affect the scaling process.

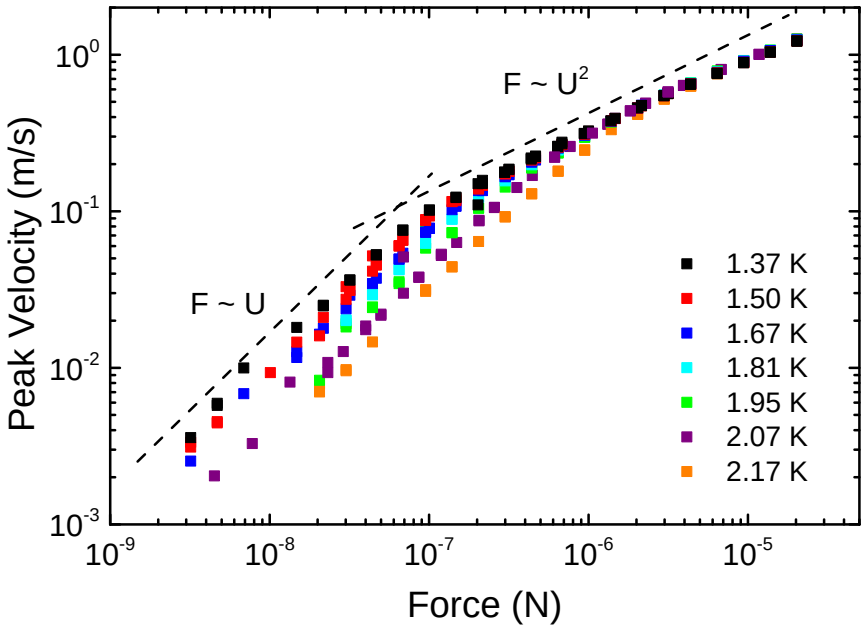

Figure 1: Plot of peak velocity U_0 against the applied force peak F_0 for the vibrating wire submerged in superfluid ^{4}He at several temperatures. The black dashed lines serve as sketch of theoretical laminar and turbulent regimes.

We plotted in **Figure (1)** the peak velocity of the wire top U_0 against the applied force peak F_0 at various temperatures from two-fluid regime ($T > 1.0\,\mathrm{K}$).

Clearly, the wire exhibits linear drag at low velocities and non-linear additional drag in the area of higher velocities. The energy losses of the wire in the low-velocity part are dominated by the viscous drag of the present normal component. Other loss mechanisms like acoustic emission are in principle present as well, but neglected in further discussion. The additional dissipation process in the higher-velocity part indicates either classical or quantum turbulence (or both) and the measured drag F_0 is roughly proportional to U_0^2.

Next we plotted in **Figure (2)** the classical drag coefficient as a function of peak force and velocity $C_D \sim F_0/U_0^2$ using the same data as presented in **Figure (1)**.

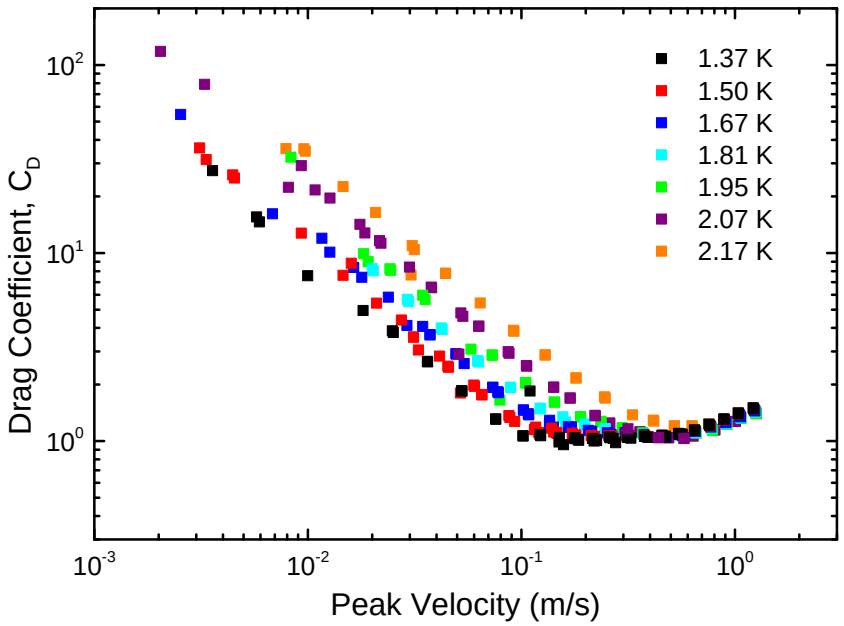

Figure 2: Plot of drag coefficient C_D against the velocity peak response U_0 for the vibrating wire at several temperatures.

In order to perform the universal scaling, we collapse the contribution of the normal component in the following way:

$$C_D^n \leftarrow C_D \frac{\rho}{\rho_n}\,, \qquad \mathrm{Dn} \leftarrow U_0 \sqrt{\frac{2\rho_n}{\eta\omega}}\,, \tag{1}$$

where η is the dynamical viscosity of Helium-II for a given temperature. Relations in (1) are performed in the same way as described (**??**), (**??**) in the last section of **Theoretical background** chapter.
The resulting plot **Figure (3)** clearly collapses all the linear parts of the measured drag.

However, the theoretical pre-factor ($\Phi_{\mathrm{cyl}} = 4\pi$) are smaller than the fitted one ($\Phi \sim 26$). This is most likely caused due to the irregularities on the surface of the wire.

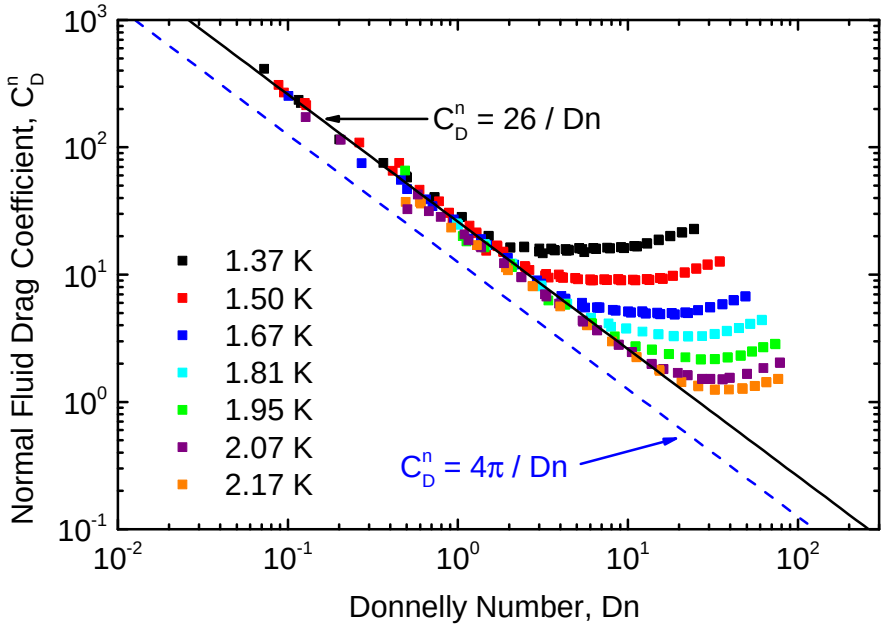

Figure 3: Plot of normal fluid drag coefficient C_D^n against the dimensionless Donnelly number (Dn) for the vibrating wire at several temperatures.The blue dashed line shows the expected theoretical dependence [4] for a smooth cylinder. The solid black line is a numerical fit of the linear part of data.
The temperature-dependent and temperature-ascending starting points of non-linearities are a clear sign of the onset of quantum turbulence by the superfluid component.

0.1.2 Oscillating disc

The (torsionally) oscillating disc differs from the vibrating wire in several technicalities:

- Oscillating disc does not displace any fluid and thus no potential flow of superfluid component is present
- It is not possible to perform measurements in a steady state of flow, but decayed flow was measured instead
- Drag force has to be measured via decaying amplitude of oscillator deflection.

As a consequence of mentioned differences (examples showed in **Figure 4**), we have to substitute $U_0 = \omega R$ within a Donnelly number and define a new drag coefficient, specific for our mechanical system of torsionally oscillating disc in a viscous fluid of density ρ_n as:

$$C_D^n \leftarrow \frac{2M_f}{A\rho_n\Omega_0^2R^3}\,, \qquad \mathrm{Dn} \leftarrow R\omega\phi_0\sqrt{\frac{2\rho_n}{\eta\omega}}\,, \tag{2}$$

where M_f is the moment of friction forces, R the radius of the disc, $A = \pi R^2$ the area of the disc and Ω_0 is the amplitude of angular velocity $\omega(t)$. It was already showed [4] the relation between such drag coefficient (2) can be expressed in laminar flow in terms of the Donnelly number as $C_D^n \sim \mathrm{Dn}$ with the pre-factor $\Phi_{\mathrm{disc}} = 2$.

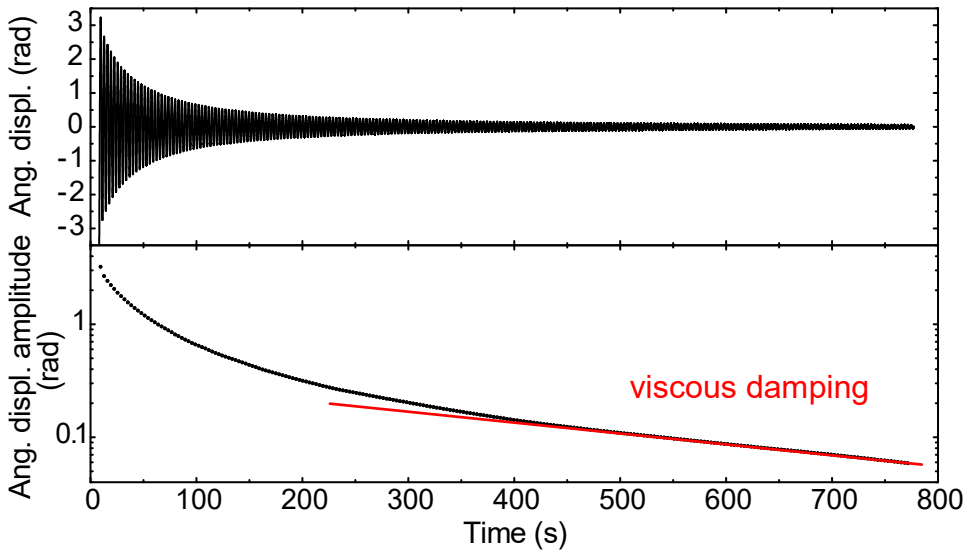

Figure 4: Example of angular displacement measurement in time of the torsionally oscillating disc. Top picture: The decreasing angular displacement amplitudes $\phi_0(t)$. Bottom picture: The logarithmic plot $\phi_0(t)$ shows two distinct regions – nonlinear decay in the area of earlier times $t < 400$ and an exponential (viscous) decay due to laminar flow of the normal component at the later times $t > 500$.

We plot the re-defined drag coefficient (2) against the Donnelly number in **Figure 5**.

Again, as in case of vibratig wire, in the area of small values of Donnelly number, the data clearly collapse to a single dependence, which illustrates the universal scaling idea. One would naturally expect the normal component to transit to turbulent regime earlier than the superfluid one since the oscillating disc directly moves only with the normal component. However, **Figure 5** clearly shows that non-linearities are not characterized by a single value of Dn, but rather continuously with ascending temperature. This implies that instabilities cannot be explained by pure viscous fluid dynamics and must relate to the quantum turbulence of vortex tangle.

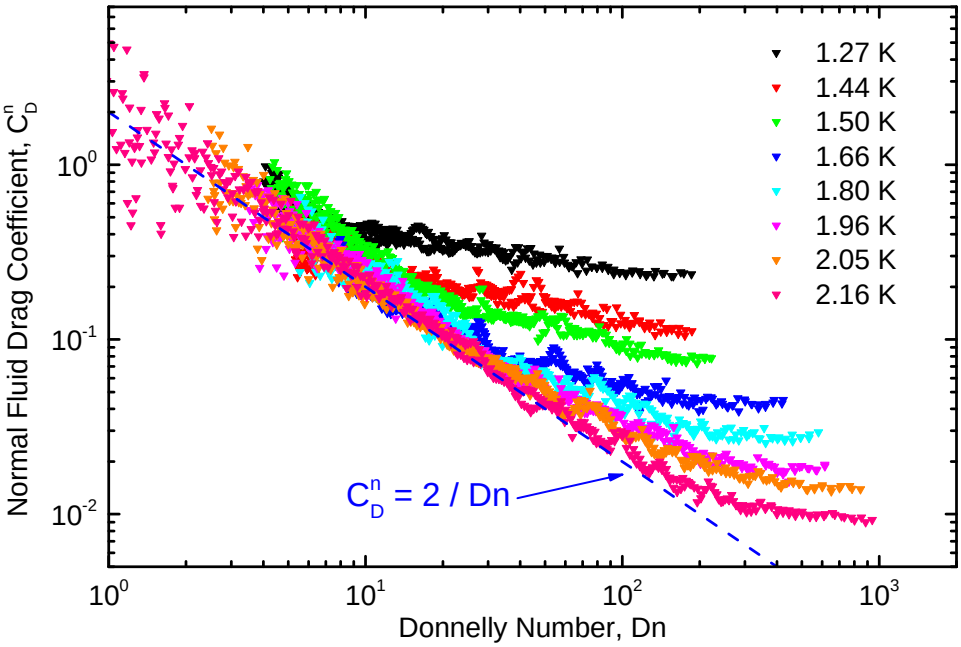

Figure 5: Plot of re-defined fluid drag coefficient C_D^n against the dimensionless Donnelly number (Dn) for the torsionally oscillating disc at several temperatures.
The blue dashed line shows the expected theoretical dependence [4] for viscous drag. The temperature-dependent and temperature-ascending starting points of non-linearities are a clear sign of the onset of quantum turbulence by the superfluid component.

Bibliography

[1] Tisza, L. *The viscosity of liquid helium and the Bose-Einstein statistics.* Comptes Rendus Acad. Sciences, **207**:1186-1189 (1952)

[2] Landau, L.D. *The theory of superfluidity of helium II* J. Phys. USSR, Vol. **11**, 91 (1947)

[3] Bahyl, J. *Measurement of quantum turbulence in superfluid He-4.* Student conference, FMPH UK, Bratislava (2016)

[4] Jackson, M.J., Schmoranzer, D., et al. *Universal Drag Force Scaling in High Stokes Number Oscillatory Flows of He II.* Phys Rev B, **submitted** (2018)

[5] Rayfield, G.W., Reif F. *Quantized Vortex Rings in Superfluid Helium* Phys. Rev. A, **136**, 5A (1964)

[6] Feynman, R. *Application of quantum mechanics to liquid helium.* Prog. in Low Temp. Phys., **1**, 17-53 (1955)

[7] Penrose, O., Onsager, L. *Bose-Einstein condensation and liquid helium.* Phys. Rev., **104**, 576 (1956)

[8] Vinen, W.F. and Hall, H.E. *The theory of mutual friction in uniformly rotating helium II.* Proc. Royal Soc. London 238 (1957) 204

[9] Donnelly, R.J., Barenghi, C.F *The Observed Properties of Liquid Helium at the Saturated Vapor Pressure.* American Ins. of Phys. and Chem. Soc. (1998)

[10] Roberts, P.H. Phys. Rev. A, 55 (1971)

[11] Donnelly, R.J. *Quantized Vortices in Helium II.* Cambridge studies in low temp. phys. (2005)

[12] Osborne, D.V. *The Rotation of Liquid Helium-II.* Proc. Royal Soc. London , **63**: 909-912 (1950)

[13] Van Dyke, M. *An Album of Fluid Motion.* The Parabolic Press, Stanford, California (1982). ISBN 0-915760-02-9

[14] Schmoranzer, D., Králová, V., et al. Phys. Rev. E, 81 (2010)

[15] Nichol, H.A., Skrbek, L. et al. Phys. Rev. Lett. **92** (2004).

[16] Holt, S., Skyba, P. Rev. Sci. Instrum., **83** (2012)

[17] Guénault, A.M., Kennedy, S.G., et al. J, of Low Temp Phys., **62** (1986)

[18] Blaauwgeers, R. Blažková, M. and col. *Quartz tuning fork: Thermometer, Pressure- and Viscometer for Helium Liquids* J. of Low Temp Phys., Vol. **146** (2007)

[19] Bradley, D.I., Človečko, M. and col. Phys. Rev. B **85** (2012)

[20] Schmoranzer, D., Jackson. M.J., et al. *Multiple critical velocities in oscillatory flow of superfluid* ^{4}He *due to quartz tuning forks.* Phys. Rev. B **94** (2010)

[21] Bahyl, J. *Measurement of Quantum Turbulence in Superfluid Helium Using Second Sound Attenuation.* Bachelor Thesis, FMPH UK, Bratislava (2016)

[22] Schwarz, K.W. *Three-dimensional vortex dynamics in superfuid He 4: Homogeneous superfluid turbulence*
Phys Rev B, Vol. **38**, 4 (1988)

[23] Tsubota, M., Fujimoto, K., Yui S. *Numerical Studies of Quantum Turbulence.* Journal of Low Temp Phys, 188 (2017)

[24] Baggaley, A.W., Barenghi, C.F. *Spectrum of turbulent Kelvin-waves cascade in superfluid helium.*
Phys Rev B, Vol. **83**, 4 (2011)

[25] Samuels, D.C. *Superfluid vortices and Turbulence.* Quantized Vortex Dynamics and Superfluid Turbulence, Chap.9 (2001)

[26] Documentation *http://docs.desktop.aero/appliedaero/potential3d/BiotSavart.html*

[27] Barenghi, F. *Superfluid vortices and Turbulence.* Quantized Vortex Dynamics and Superfluid Turbulence, Chap.1 (2001)

[28] Baggaley, A.W., Barenghi, C.F. *Tree Method for Quantum Vortex Dynamics.* Journal of Low Temp Phys, 166 (2012)

[29] Barnes, J., Hut, P. *A hierarchical O(N log N) force-calculation algorithm.* Nature, **324**, 446 (1986)